Papers in Natural Resources   Natural Resources, School of

1-20-2005

Effect of Bio-Optical Parameter Variability on the Remote Estimation of Chlorophyll-a Concentration in Turbid Productive Waters: Experimental Results

Giorgio Dall'Olmo
Oregon State University, giorgiod@science.oregonstate.edu

Anatoly A. Gitelson
University of Nebraska - Lincoln, agitelson2@unl.edu

Effect of bio-optical parameter variability on the remote estimation of chlorophyll-a concentration in turbid productive waters: experimental results

Giorgio Dall'Olmo and Anatoly A. Gitelson

The analytical development and underlying hypothesis of a three-band algorithm for estimating chlorophyll-a concentration ([Chla]) in turbid productive waters are presented. The sensitivity of the algorithm to the spectral location of the bands used is analyzed. A large set of experimental observations ([Chla] varied between 4 and 217 mg m^{-3} and turbidity between 2 and 78 nephelometric turbidity units) was used to calibrate and validate the algorithm. It was found that the variability of the chlorophyll-a fluorescence quantum yield and of the chlorophyll-a specific absorption coefficient can reduce considerably the accuracy of remote predictions of [Chla]. Instead of parameterizing these interferences, their effects were minimized by tuning the spectral regions used in the algorithm. This allowed us to predict [Chla] with a relative root-mean-square error of less than 30%.   © 2005 Optical Society of America

OCIS codes: 010.4450, 280.0280.

1. Introduction

Satellite and airborne optical sensors can provide the high spatial and temporal resolution data that are needed for monitoring inland and coastal water ecosystems. The radiance signals recorded remotely in specific regions of the electromagnetic spectrum are usually transformed into reflectance and combined into models for the remote estimation of chlorophyll-a concentration, [Chla], a parameter that is relatable to the biomass and productivity of phytoplankton.

In turbid productive waters, two main categories of models are used: (a) combinations of reflectance bands (usually band ratios) that exploit the absorption band of chlorophyll-a (Chla) in the red spectral region[1–7]; and (b) algorithms that use the Chla fluorescence emission at 685 nm (Refs. 8–11). These models are based on different assumptions, among which are the constancy of optical parameters such as the Chla specific absorption coefficient, $a_{Chla}*$, and the Chla fluorescence quantum yield, η. These parame-

ters, in practice, are variable and depend on the physiological and ecological dynamics of the phytoplankton community. For example, for [Chla] values between 0.02 and 25 mg m^{-3}, Bricaud *et al.*[12] have shown that $a_{Chla}*(675)$ can vary up to fourfold. Furthermore, η depends on several factors such as phytoplankton taxonomic composition, illumination conditions, nutritional status, and temperature, and can vary by up to a factor of 8.[13,14] Therefore the assumptions of constant $a_{Chla}*$ and η can be a significant source of uncertainty in models for the remote estimation of [Chla].

Recently, Dall'Olmo *et al.*[15] provided empirical evidence demonstrating that a three-band reflectance model, originally developed for estimating Chla amounts in terrestrial vegetation,[16] could be also used for assessing [Chla] in turbid productive waters. The objectives of this paper are as follow: (1) to present the analytical development and the underlying hypothesis behind the above algorithm; (2) to analyze the sensitivity of the proposed model to the spectral locations of the bands used; (3) to assess the performances of the proposed and existing algorithms.

We show that, in specific spectral regions, the accuracy of the algorithm is maximally affected by interferences owing to the variability of the Chla fluorescence quantum yield and of the Chla specific absorption coefficient. We also show how to deter-

G. Dall'Olmo (gdall@calmit.unl.edu) and A. A. Gitelson are with the Center for Advanced Land Management Information Technologies, School of Natural Resources, University of Nebraska-Lincoln, 113 Nebraska Hall, Lincoln, Nebraska 68588-0517.

mine the spectral regions that minimize the uncertainty in [Chla] estimation. The data set that was used in this analysis encompasses a large part of the natural seasonal and interannual variability of [Chla], a_{Chla}^*, and η of inland turbid productive waters and finally allows us to establish statistically robust relationships between remote sensing models and [Chla] measured analytically.

2. Algorithm Development

Spectral remote-sensing reflectance, $R_{rs}(\lambda, \theta, \phi)$, is defined as the ratio of water leaving radiance, $L_u(0^+, \lambda, \theta, \phi)$, to downward irradiance, $E_d(0^+, \lambda)$, both measured above the water surface and as a function of wavelength, λ; θ and ϕ are the viewing zenith and azimuth angles, respectively. In an homogeneous water body, $R_{rs}(\lambda, \theta, \phi)$ can be expressed in terms of the inherent optical properties, total absorption (a) and backscattering (b_b) coefficients, as follows[17–19]:

$$R_{rs}(\lambda, \theta, \phi) \propto \frac{f(\lambda, \theta_w, \phi_w)}{Q(\lambda, \theta_w, \phi_w)} \frac{b_b(\lambda)}{a(\lambda) + b_b(\lambda)}, \quad (1)$$

where $f(\lambda, \theta_w, \phi_w)$ is a coefficient dependent on the Sun zenith angle and on the volume scattering function of the medium[20]; $Q(\lambda, \theta_w, \phi_w) = E_u(0^-, \lambda)/L_u(0^-, \lambda, \theta_w, \phi_w)$, $E_u(0^-, \lambda)$, and $L_u(0^-, \lambda, \theta_w, \phi_w)$ are the below-surface upwelling irradiance and radiance, respectively; θ_w and ϕ_w are in-water zenith and azimuth viewing angles, respectively.[21] Hereinafter, we consider all the radiometric quantities dependent on viewing angle as measured at nadir; thus we drop the arguments referring to the angular dependency.

The $f(\lambda)/Q(\lambda)$ ratio describes the dependence of $R_{rs}(\lambda)$ on the geometry of the light field emerging from the water body. Its spectral variations with Sun and viewing geometry are related to the average number of scattering events experienced by photons of wavelength λ before emerging from the water, $\bar{n}(\lambda) = 1 + b(\lambda)/a(\lambda)$, where b is the total scattering coefficient.[20] In turbid productive waters ([Chla] in the range 10–100 mg m^{-3}), typical values of $\bar{n}$ between 650 and 750 nm, range approximately from 3 to 9. For this range of $\bar{n}$ and for the Sun at zenith and a sensor viewing in the nadir direction, the $f(\lambda)/Q(\lambda)$ ratio changes at maximum by approximately 20% (Fig. 9 of Ref. 22). For other viewing angles in the remote-sensing domain ($\theta_w < 35°$, Ref. 22) and a solar zenith angle of 60°, similar results can be expected.[22] Thus as a first approximation, we assumed that the $f(\lambda)/Q(\lambda)$ ratio is spectrally invariant in the range 650–750 nm. We also assumed that the total backscattering coefficient, $b_b(\lambda)$, is invariant in the same spectral range.[5,23,24] Therefore from this point on, we omit the argument λ from these quantities. Finally, we considered the absorption coefficient of water, a_w, independent of temperature.

Because of the overlapping absorption by chromophoric dissolved organic matter (CDOM), tripton, and phytoplankton pigments in the blue-green spectral region, to extract information on [Chla], we exploited the Chla red-absorption maximum around 675 nm. In order to obtain a function directly related to Chla absorption, we used the reciprocal of R_{rs}:

$$R_{rs}^{-1}(\lambda_1) \propto \frac{Q}{f} \frac{a_{Chla}(\lambda_1) + a_{TD}(\lambda_1) + a_w(\lambda_1) + b_b}{b_b}, \quad (2)$$

where a_{Chla} is the Chla absorption coefficient, $a_{TD} = a_{CDOM} + a_{tripton}$, and a_{CDOM} and $a_{tripton}$ are the absorption coefficients of CDOM and tripton (non-algal particles), respectively. λ_1 is the first spectral region selected to have $R_{rs}(\lambda_1)$ maximally sensitive to a_{Chla}, i.e., $660 \leq \lambda_1 \leq 690$ nm.

We aimed at isolating $a_{Chla}(\lambda_1)$ from relation (2) by minimizing the effects of b_b and $a_{TD}(\lambda_1)$, using R_{rs} at two wavelengths different from λ_1. To remove b_b and $a_{TD}(\lambda_1)$ from the numerator of relation (2), we selected a second spectral region λ_2 such that $a_{TD}(\lambda_1) \sim a_{TD}(\lambda_2)$, and $a_{Chla}(\lambda_1) \gg a_{Chla}(\lambda_2)$. Considering the exponential decrease of the absorption coefficients of CDOM and detritus toward longer wavelengths,[25,26] and the likely effect of the absorption by accessory pigments (e.g., chlorophyll-b) on R_{rs} at $\lambda < 660$ nm, we expected to find λ_2 beyond 700 nm. By subtracting $R_{rs}^{-1}(\lambda_2)$ from $R_{rs}^{-1}(\lambda_1)$, we therefore removed b_b and $a_{TD}(\lambda_1)$ from the numerator of Eq. (2), obtaining

$$R_{rs}^{-1}(\lambda_1) - R_{rs}^{-1}(\lambda_2) \propto \frac{Q}{f} \frac{a_{Chla}(\lambda_1) + a_w(\lambda_1) - a_w(\lambda_2)}{b_b}. \quad (3)$$

Note that, by assuming an average exponential slope of a_{TD} of -0.01, one obtains $a_{TD}(675)/a_{TD}(700) \sim 1.3$. However, this uncertainty can be considered negligible since a_{TD} values in this spectral region are relatively low (e.g., Ref. 27).

To remove b_b and Q/f from relation (3), we selected a third spectral region λ_3, where $a_{Chla}(\lambda_3) + a_{TD}(\lambda_3) \sim 0$, and thus $a(\lambda_3) \sim a_w(\lambda_3) \sim$ constant (under our assumptions). Such a spectral region can be found in the near-infrared (NIR) range (i.e., $\lambda_3 > 730$ nm).[5,28] In the NIR, $a \gg b_b$; thus reflectance in this region can be approximated as

$$R_{rs}(\lambda_3) \propto \frac{f}{Q} b_b. \quad (4)$$

Multiplying relation (3) and relation (4), we obtain

$$[R_{rs}^{-1}(\lambda_1) - R_{rs}^{-1}(\lambda_2)]R_{rs}(\lambda_3) \propto a_{Chla}(\lambda_1). \quad (5)$$

Thus by selecting three appropriate spectral regions λ_1, λ_2, and λ_3, it appears possible to isolate the Chla absorption coefficient at λ_1 from R_{rs}. We can then use Beer's law to relate [Chla] with the function $[R_{rs}^{-1}(\lambda_1) - R_{rs}^{-1}(\lambda_2)]R_{rs}(\lambda_3)$.

If $a_{TD}(\lambda_1) \ll a_{Chla}(\lambda_1)$ and $b_b \ll a(\lambda_1)$, then, by multiplying relations (2) and (4), we obtain a special case

of relation (5):

$$R_{rs}^{-1}(\lambda_1)R_{rs}(\lambda_3) \propto a_{Chla}(\lambda_1). \qquad (6)$$

Equation (6) relates a_{Chla} to the NIR-to-red reflectance ratios that are widely used for the remote estimation of [Chla] in turbid productive waters.[1–8] For the sake of brevity, we indicate hereinafter the left-hand sides of relations (5) and (6) as Y and Z, respectively.

3. Methodology

We sampled two complementary types of Eastern Nebraska water bodies, typical of this agriculturally dominated region: sand pit lakes (Fremont State Lakes and Ginger Cove), in which the suspended material is mainly of organic origin, and reservoirs (Glen Cunningham and Branched Oak), with a gradient of inorganic suspended material from the inlet to the dam. Data were collected during 19 campaigns, from June 2001 to October 2001 and from May 2002 to October 2002. We also included in the data set 16 stations collected at Lake Okoboji, Iowa, on 30 September 2002. This is a lake of glacial origin that is divided into two subbasins: the East Okoboji, which is shallow, turbid, and eutrophic, and the West Okoboji, which is deeper and mesotrophic.

A. Field Measurements

Hyperspectral reflectance measurements were taken from a boat using two intercalibrated Ocean Optics USB2000 radiometers. Data were collected in the range 400–900 nm with a sampling interval of 0.3 nm and a spectral resolution of ~ 1.5 nm. Radiometer 1, equipped with a 25° field-of-view optical fiber, was pointed downward to measure the below-surface nadir upward radiance, $L_u(0^-, \lambda)$. The tip of the optical fiber was kept just below the water surface, on the sunny side of the boat, by means of a 2-m handheld black beam. Interferences in the light field were considered negligible owing to the small diameter (~ 0.5 cm) of the tip of the optical fiber and of the high turbidity of these waters. Most of the lakes sampled had rather short fetches (of the order of tens of meters) and were protected by trees; thus, even under windy conditions, waves were almost absent. Only in the larger Lake Okoboji (with a fetch of the order of hundreds of meters), owing to waves, the tip of the optical fiber was kept at a deeper depth (approximately 15–30 cm). Radiometer 2 was equipped with an optical fiber and a cosine collector that was pointed upward, by means of another beam fixed to the boat, to measure the above-surface downward irradiance, $E_u(0^+, \lambda)$. The integration time of radiometer 2 was usually approximately 10 times shorter than that of radiometer 1. However, provided the variations in illumination conditions can be considered negligible during the short time taken to collect one measurement (~ 30 seconds), the data recorded by radiometer 2 were considered representative of the overall downward irradiance. Solar zenith angle

ranged from approximately 55° to a maximum of 20°. All measurements were taken over optically deep water.

The digital numbers (DNs) produced by the radiometers can be expressed as follows (the λ notation has been omitted for simplicity):

$$DN_L = L_u(0^-)k_L, \qquad (7a)$$

$$DN_E = E_d(0^+)k_E, \qquad (7b)$$

where k is a transformation coefficient, specific to each radiometer, and the subscripts L and E stand for upward nadir radiance and downward irradiance, respectively.

The first 25 elements of the USB2000 detector array are screened from light energy and therefore record a signal owing to the dark current of the instrument. For each scan, they were used to estimate an average value of dark current that was then subtracted from the raw digital numbers. Hereinafter, this correction is considered applied and is not indicated.

The ratio of Eqs. (7a) and (7b) yields the quantity $DN_L/DN_E = L_u(0^-)/E_d(0^+)(k_L/k_E)$, which depends on the radiance reflectance of the target, but also on the ratio of the transformation coefficients of the two instruments, k_L/k_E. To evaluate k_L/k_E and to assess its stability with time, we used a white Spectralon panel of known irradiance reflectance, R_{ref}. By collecting measurements on the reference panel, we computed $k_L/k_E = (DN_{L,\,ref}/DN_{E,\,ref})/(R_{ref}/\pi)$, where $DN_{L,\,ref}$ and $DN_{E,\,ref}$ are the digital numbers recorded by the downward and upward looking radiometers, respectively, while scanning the Spectralon panel; the factor π is introduced to transform the irradiance reflectance R_{ref} into a radiance reflectance (assuming that the reference Spectralon panel is a Lambertian reflector). The above-water remote-sensing reflectance of the target was finally computed as

$$R_{rs} = \frac{DN_L}{DN_E} \frac{DN_{ref,E}}{DN_{ref,L}} \frac{R_{ref}}{\pi} \frac{t}{n^2} F_i, \qquad (8)$$

where t is the radiance transmittance from water to air (~ 0.98, Ref. 29), n is the refractive index of water (~ 1.33), and F_i is the spectral immersion factor.

We carried out laboratory experiments to assess the variability of k_L/k_E with time. The coefficient of variation of k_L/k_E did not exceed 2% over a period of four hours (Dall'Olmo 2001, unpublished data), therefore supporting the stability of our measurement system. Because k_L/k_E may change among field campaigns owing to unscrewing or rearranging of fiber optics and/or cosine collector, k_L/k_E was measured at least twice during each field campaign. Relation (8) was then evaluated using the median value of $DN_{ref,E}/DN_{ref,L}$.

Traditionally, reflectance measurements are collected either by means of two absolutely calibrated radiometers (one measuring the upward radiation from the target and the other measuring the downward irradiance), or by using a single radiometer and subsequently collecting measurements over a panel of known reflectance and over the target. The methodology that was adopted in this study was advantageous because it allowed us to collect data under variable illumination conditions (usually prohibitive for the single-instrument technique) without requiring absolute calibration of the radiometers.

At each station, six reflectance spectra were measured, each averaging 15 consecutive scans. These six spectra were then smoothed using a moving average (window size of 5 nm), interpolated every nanometer, and the median spectrum was computed for further analysis.

At each station, Secchi disk depth and turbidity (using a portable Hach 2100 turbidimeter) were measured, and surface water (0.5 m) was collected and stored in the dark in a cooler with ice. Samples were filtered on Pall Gellman type A/E glass fiber filters and frozen for successive laboratory analyses.

B. Laboratory Measurements

Chlorophyll-a was extracted in hot ethanol, and its concentration was quantified fluorometrically.[30] The concentrations of total (TSS), organic (OSS), and inorganic suspended solids (ISS) were determined gravimetrically.[31] Spectral absorption measurements of constituents on filters were carried out in 2002 immediately after every field campaign with a Cary 100 Varian spectrophotometer. The optical densities of total suspended particles and tripton (after oxidation of pigments by means of diluted chlorine water[32]) were measured on filters (Whatman GF/F)[33] and corrected for scattering by subtracting the optical density at 750 nm from the entire spectrum. Conversion of optical densities into absorption coefficients was accomplished by using published coefficients.[34] Pigment absorption coefficients were computed as the difference between total particle and tripton absorption coefficients. By adjusting the sample volume filtered, we kept the optical density of filters at 440 nm between 0.2 and 0.5. The CDOM absorption coefficients were measured as in Bricaud *et al.*[26]

4. Results and Discussion

A. Data Set Description

The data set encompasses variable optical conditions and includes a wide range of phytoplankton taxonomic groups (Chrysophyta, Chlorophyta, Cyanophyta, Cryptophyta, Pyrrophyta). [Chla], Secchi disk depth, turbidity, and the absorption coefficients of CDOM and tripton at 440 nm spanned over two orders of magnitude, while TSS, OSS and ISS spanned over three orders of magnitude (Table 1). Absorption by Chla at 678 nm, $a_{Chla}(678)$, ranged from 0.1 m^{-1} to 6.0 m^{-1} with an average value of 1.0 m^{-1}. The sum of the absorption coefficients by CDOM and tripton at

Table 1. Descriptive Statistics of the Optical Water Quality Parameters Measured[a]

	Mean	St. Dev.	Median	Min	Max	N
[Chla], mg m^{-3}	46.5	41.4	36.1	4.4	217.3	144
Secchi disk depth, cm	80.9	57.0	63.0	18.0	299.0	138
Turbidity, NTU	20.1	15.7	16.9	1.7	78.0	135
TSS, mg L^{-1}	18.9	19.6	14.0	0.2	166.4	130
ISS, mg L^{-1}	8.0	15.6	2.6	<0.1	139.8	130
OSS, mg L^{-1}	10.9	7.9	10.0	0.2	48.2	130
$a_{CDOM}(440)$, m^{-1}	1.2	0.7	1.0	0.5	4.4	101
$a_{tripton}(440)$, m^{-1}	2.2	1.3	2.0	0.4	6.7	102
$a_{Chla}(678)$, m^{-1}	1.0	0.8	1.0	0.1	6.0	102
$a_{TD}(678)$, m^{-1}	0.18	0.09	0.15	0.04	0.48	101

[a]TSS, total suspended solids; ISS, inorganic suspended solids; OSS, organic suspended solids; $a_{CDOM}(440)$, absorption coefficient of CDOM at 440 nm; $a_{tripton}(440)$, absorption coefficient of tripton at 440 nm; $a_{Chla}(678)$, absorption coefficient of Chla at 678 nm; $a_{TD}(678)$, sum of the absorption coefficients of tripton and CDOM at 678 nm; N, number of samples.

678 nm, $a_{TD}(678)$, ranged from 0.04 to 0.48 m^{-1} with an average value of 0.18 m^{-1}, thus being one order of magnitude lower than $a_{Chla}(678)$. $a_{CDOM}(440)$, $a_{tripton}(440)$, TSS, and ISS correlated weakly with [Chla] (see Fig. 1), confirming that the water bodies sampled belong to case 2 waters.[35]

Remote-sensing reflectance spectra varied largely over the visible and NIR spectral regions (Fig. 2). These spectra are comparable both in shape and magnitude to others collected in turbid productive wa-
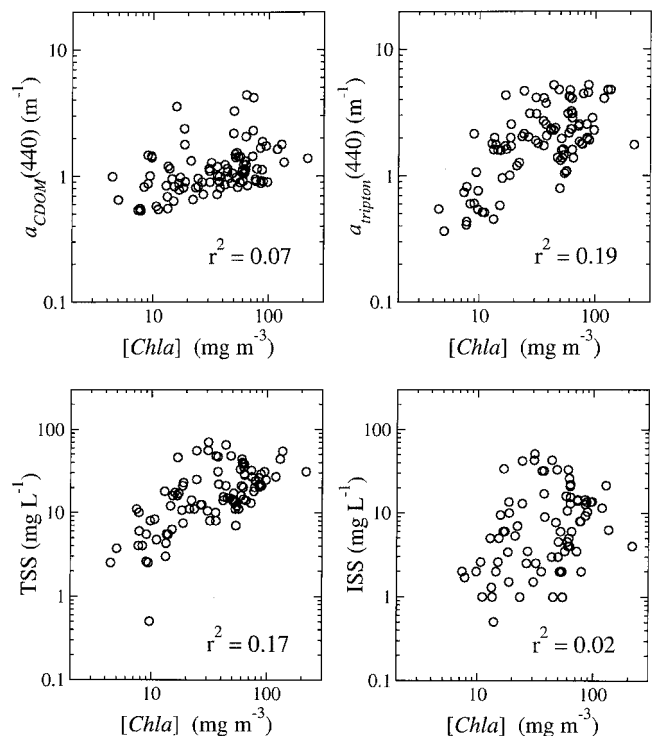

Fig. 1. Relationships between [Chla] and other "optically active" constituents indicating that the lakes studied belong to case 2 waters. Determination coefficients for linear relationships are presented in each plot.
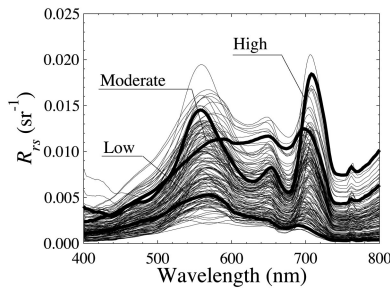
Fig. 2. Remote-sensing reflectance spectra of the water bodies studied. Some examples are highlighted: curve "Low," [Chla] = 11 mg m^{-3}, TSS = 5 mg L^{-1}; curve "High," [Chla] = 89 mg m^{-3}, TSS = 21 mg L^{-1}; curve "Moderate," [Chla] = 24 mg m^{-3}, TSS = 55 mg L^{-1}.

Fig. 4. Chla specific absorption coefficient at 678 nm as a function of [Chla].

ters.[17] They were characterized by (1) minimal values in the blue region (400–500 nm) owing to the combined absorption by phytoplankton pigments, CDOM, and tripton; (2) a peak in the green region (~550 nm) owing to minimal values of total absorption; (3) a minimum in the red region (~675 nm) owing to Chla absorption; (4) a local maximum in the range 690–715 nm owing to a minimum in total absorption;[36,37] (5) lower values in the NIR region (>750 nm) owing to high absorption by pure water. Specifically, $R_{rs}(750)$ varied from 0.0002 to 0.0076 sr^{-1}, indicating a wide range of scattering regimes sampled. As an example, we highlighted in Fig. 2 three spectra, typical of low Chla concentrations ([Chla] = 11 mg m^{-3}, TSS = 5 mg L^{-1}, curve "low"), high Chla concentrations ([Chla] = 89 mg m^{-3}, TSS = 21 mg L^{-1}, curve "high"), and moderate Chla concentrations and high TSS ([Chla] = 24 mg m^{-3}, TSS = 55 mg L^{-1}, curve "moderate"). Importantly, despite Sun-induced Chla, fluorescence manifests itself in reflectance spectra through a local maximum around 685 nm;[38,39] the position of the reflectance maximum was always found at longer wavelengths, between 690 and 715 nm (Fig. 3).

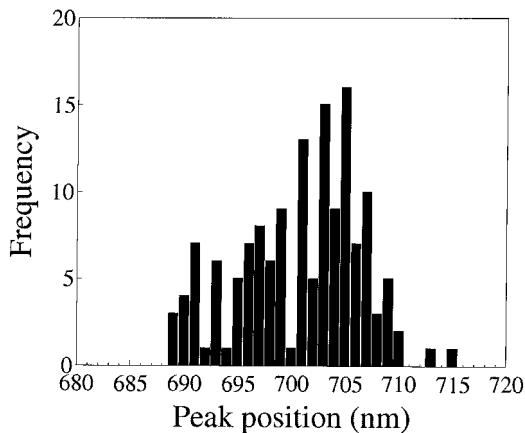The Chla specific absorption coefficient at 678 nm, $a_{Chla}*(678)$, showed a weak inverse relationship with

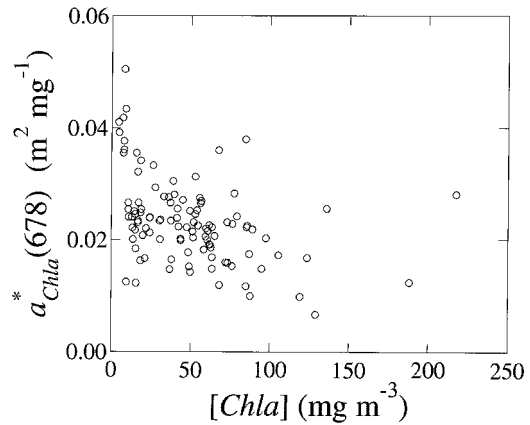Fig. 3. Frequency distribution of the position of the reflectance maximum around 700 nm.

[Chla], similar to those already reported in literature for this range of [Chla] values[12,40] (Fig. 4); it ranged between 0.005 and 0.050 m^2 mg^{-1} with a median of 0.023 m^2 mg^{-1}. These values are comparable with published data (e.g., Refs. 12 and 40–42), but appear to be larger than those presented in other studied (e.g., Refs. 43 and 44). Even though one cannot ignore uncertainties introduced by the filter pad method and by the Chla extraction technique, the variability of the presented $a_{Chla}*(678)$ values can be related to changes in the packaging effect owing to the wide range of phytoplankton groups and environmental conditions sampled.

We calculated the average number of photon collision $\bar{n}$ using the 1-to-1 relationship between nephelometric turbidity units (NTUs) and b (see Kirk[27] and references therein). At 570 nm (the spectral region where the sensitivity of the portable Hach 2100 turbidimeter is maximal), $\bar{n}$ spanned from 5.5 to 54.4 with a median value of 20.7. Assuming that $b(570) \sim b(678)$, we also computed $\bar{n}(678)$, which spanned from 2.3 to 44.5 with a median value of 12.1. Therefore multiple scattering prevailed in the water bodies sampled; furthermore, the range of $\bar{n}$ found is consistent with that used for our hypothesis concerning the spectral independency of f/Q.

B. Algorithm Calibration

The calibration of relations (5) and (6) for the quantification of [Chla] requires two steps: (a) the identification of the optimal λ_1, λ_2, and λ_3; and (b) the parameterization of the relationships between Y and Z, and [Chla]. To calibrate and validate the models, the data set was divided into two independent subsets as follows. The calibration data set ($N = 86$) was assembled by using data collected in the Fremont State Lakes, Lake Okoboji, and Ginger Cove during 2002. Moreover, to balance the number of stations collected in sand pit lakes and reservoirs, we added the stations collected in Branched Oak Reservoir during June and July 2002. The validation data set ($N = 58$) was composed of the remaining data: the stations collected in Fremont State Lakes and Glen Cun-

ningham during 2001 and those collected in Branched Oak Reservoir during August, September, and October 2002.

1. Tuning of the Spectral Regions

To determine the optimal spectral regions λ_1, λ_2, and λ_3 to be used in Y and Z for estimating [Chla], we adopted a stepwise technique based on linear regressions of different model versions versus [Chla] measured analytically. Based on the rationale behind the model development, we adopted the following initial spectral regions: $\lambda_1^0 = 675$ nm, $\lambda_2^0 = 710$ nm, and $\lambda_3^0 = 750$ nm.

To estimate the optimal λ_1, using the initial λ_2^0 and λ_3^0, we linearly regressed the model $[R_{rs}^{-1}(\lambda_1) - R_{rs}^{-1}(715)]R_{rs}(750)$ versus [Chla], for each value of λ_1 between 400 and 800 nm. We computed the regression standard error (STE) of estimate and obtained a narrow minimum of STE centered at $\lambda_1 = 671$ nm [Fig. 5(a)]. Thus we selected $\lambda_1 = 671$ nm.

To determine the optimal λ_2, using the optimal λ_1 and initial λ_3^0, we then regressed the model $[R_{rs}^{-1}(671) - R_{rs}^{-1}(\lambda_2)]R_{rs}(750)$ versus [Chla]. The STE was characterized by a broad minimum spanning from 700 to 750 nm [Fig. 5(b)]. To keep the sensitivity of Y with respect to [Chla] high, we selected as optimal $\lambda_2 = 710$ nm.

Finally, to identify the optimal λ_3, using the optimal λ_1 and λ_2, we regressed the model $[R_{rs}^{-1}(671) - R_{rs}^{-1}(710)]R_{rs}(\lambda_3)$ versus [Chla]. The minimum of STE was located between 730 and 750 nm [Fig. 5(c)]. We selected the optimal λ_3 in the middle of that range, i.e., $\lambda_3 = 740$ nm.

To verify that the above procedure does not depend on the initial values of λ_1, λ_2, and λ_3, we reassessed the optimal λ_1 after setting $\lambda_2 = 710$ nm and $\lambda_3 = 740$ nm. The result of this computation is the dashed curve in Fig. 5(a). The almost complete overlapping with the initial solid curve in the minim region supports the robustness of the adopted tuning methodology.

Interestingly, the range of the optimal spectral regions for λ_2 and λ_3 overlapped, i.e., $\lambda_2 = \lambda_3$, between 730 and 750 nm. Since $R_{rs}^{-1}(\lambda_2)$ is used to account for variations in the absorption by tripton and CDOM as well as in backscattering, and $R_{rs}(\lambda_3)$ is used to account for variations in backscattering only, it became clear that, for this data set, the effect of the variability of the total backscattering coefficient on reflectance was greater than that owing to the variability of a_{TD}. Our data confirm this reasoning: While $a_{TD}(678)$ varied twelvefold, $R_{rs}(750)$ varied 45-fold. The variability in $R_{rs}(750)$ can be considered mostly due to variations in b_b. At this wavelength, changes in R_{rs} from other factors are smaller: Variations in R_{rs} owing to variations in f/Q (for $\bar{n}$ changing from 3 to 61) or in a_w (for a 20 °C change in water temperature) can be approximately as high as a factor of 1% and 10%, respectively.[22,45]
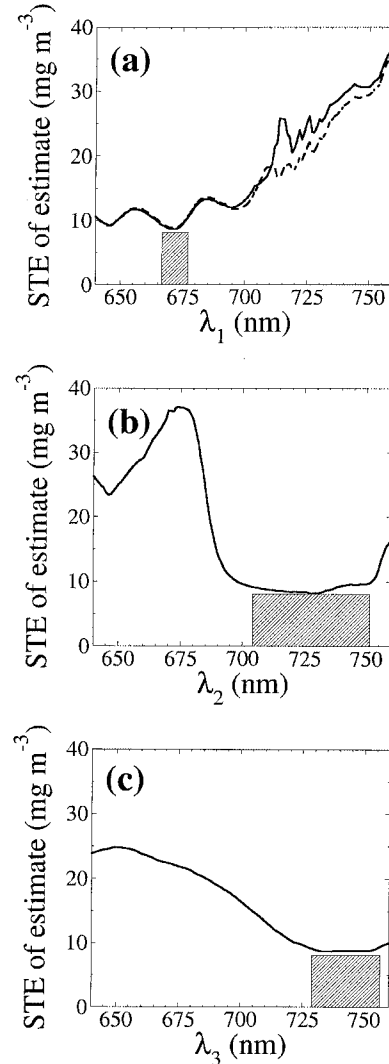

Fig. 5. STE of estimate resulting from regressing different model versions versus [Chla] measured analytically: (a) $[R_{rs}^{-1}(\lambda_1) - R_{rs}^{-1}(715)]R_{rs}(750)$ letting vary λ_1, (b) $[R_{rs}^{-1}(671) - R_{rs}^{-1}(\lambda_2)] \times R_{rs}(750)$ letting vary λ_2, and (c) $[R_{rs}^{-1}(671) - R_{rs}^{-1}(710)] \times R_{rs}(\lambda_3)$ letting vary λ_3. Boxes indicate the spectral regions where the STE was minimal. The dashed curve in plot (a) represents the STE for the model $[R_{rs}^{-1}(\lambda_1) - R_{rs}^{-1}(710)]R_{rs}(740)$ that was used to verify the tuning procedure.

2. Algorithm Sensitivity to Band Positions

To analyze the sensitivity of Y and Z to the positions of both λ_1 and λ_3, we computed STE of estimate of the linear regressions for both Y (with λ_2 fixed at 710 nm) and Z, for $650 \leq \lambda_1 \leq 700$ nm, and $700 \leq \lambda_3 \leq 750$ nm. For both models, the STE had a minimum at λ_1 between 660 and 673 nm and a maximum around 685 nm [Figs. 6(a) and (b)]. When λ_3 decreased from 750 to 700 nm, the local maximum around 685 nm gradually became more pronounced, and the minimum STE shifted from $\lambda_1 \sim 673$ nm toward shorter wavelengths [Figs. 6(a) and (b)]. In addition, as λ_3 shifted toward 750 nm, while the STE of Y decreased to a minimum value that was reached at $\lambda_3 = 730$ nm, the STE of Z decreased to a minimum
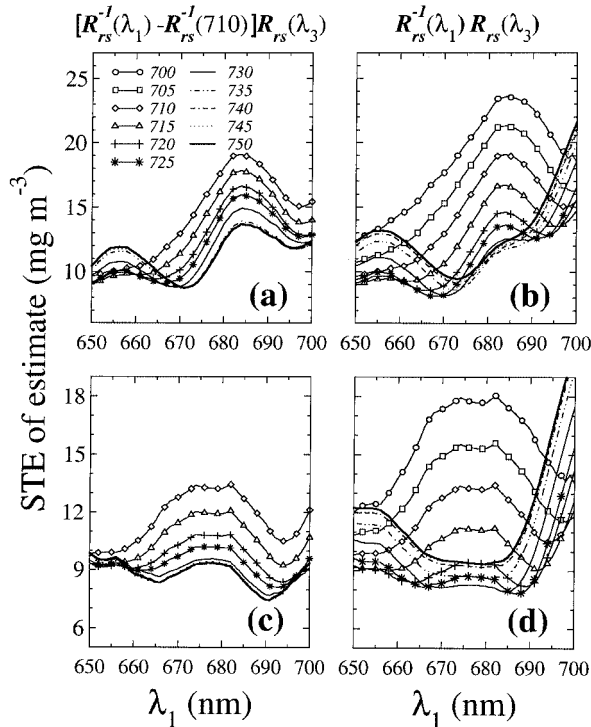
Fig. 6. STE of estimate for models Y (left column) and Z (right column) as a function of λ_1 and λ_3: (a), (b) all data shown; (c), (d) spectra with red reflectance minimum at $\lambda < 675$ nm were excluded. Numbers in legend refer to the values of λ_3. For model Y, we used $\lambda_2 = 710$ nm; thus only $\lambda_3 \geq 710$ nm were considered. Note the change of scale on the ordinate axis between plots on first and second rows.
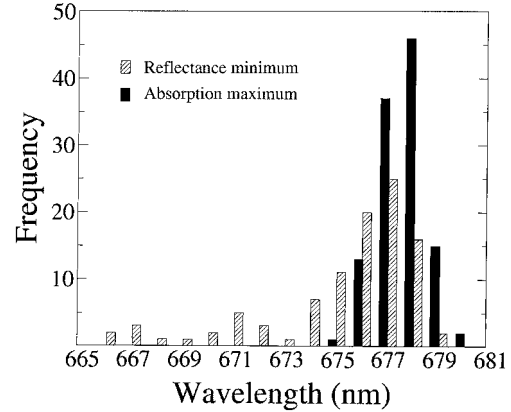

Fig. 7. Frequency distribution of the positions of the pigment red-absorption maximum measured in laboratory (using monochromatic light) and of the corresponding minimum of reflectance measured in the field.

for $\lambda_3 = 725$ nm and then begun to increase, indicating that, by using the three band model, one can exploit the NIR spectral region >730 nm.

The λ_1 region of maximal sensitivity of Z with respect to [Chla] is expected to be at $\lambda_1 \sim 675$ nm (Refs. 1–3, 8). Yet, when λ_3 was located between 700 and 730 nm, the optimal positions of λ_1 for our experimental data were located at shorter wavelengths ($657 < \lambda_1 < 673$ nm). Chla fluorescence emission peaks at 685 nm; thus the maximum of STE of estimate [Figs. 6(a) and (b)] can be explained by the variability of the Chla fluorescence quantum yield among samples that is not accounted for by the models Y and Z. For λ_3 around 700 nm, the interference was maximal and the minimum STE of estimate was found at λ_1 around 660 nm. As λ_3 shifted toward longer wavelengths, the interference became less important, and the optimal λ_1 was found around 673 nm.

To reveal the effect of Sun-induced Chla fluorescence on the reflectance spectra, we compared the position of the minimum around 675 nm in the reflectance spectra collected in the field to the corresponding position of the red maximum of the pigment absorption spectra measured in the lab. Note that absorption spectra were measured using monochromatic light, thus minimizing the contribution of Chla fluorescence. On the contrary, reflectance spectra

were collected under sunlight that provided the excitation energy for Chla fluorescence. The distribution of the positions of the absorption maximum was centered around 678 nm and symmetrically distributed in a narrow range from 675 to 680 nm (Fig. 7). On the other hand, the distribution of the position of the reflectance minimum was negatively skewed with minimum and maximum values at 666 and 679 nm, respectively. Thus in some samples, the reflectance minimum shifted up to 11 nm toward shorter wavelengths with respect to the corresponding absorption maximum. We attribute this shift to the superimposition of the Sun-induced Chla fluorescence signal that fills in the reflectance trough around 675 nm therefore shifting the reflectance minimum toward shorter wavelengths.[46,47]

To gain some insight on the importance of the interferences owing to variations in the specific absorption coefficient, we attempted to isolate the effect of this factor from the effect of fluorescence. On the basis of Fig. 7, we removed from the development data set all reflectance spectra that displayed a minimum at a wavelength shorter than 675 nm (26 stations were eliminated from the initial 86) and again computed the linear-regression STE of estimate for both Y and Z for $650 \leq \lambda_1 \leq 700$ nm and $700 \leq \lambda_3 \leq 750$ nm. Beside the maximum of STE around 685 nm, another STE peak appeared around 675 nm [compare Figs. 6(a) with 6(c), and 6(b) with 6(d)]. The different spectral shapes of the STE can be interpreted as an increase in the relative importance of the interferences owing to the packaging effect. However, some residual interferences by Chla fluorescence remained. Since, using all the reflectance spectra, we obtained a distinct peak of STE centered at 685 nm [Figs. 6(a) and 6(b)], we concluded that, for this data set, the most important of the two interfering factors considered was the variability of the Chla fluorescence quantum yield. We may anticipate that different results might be obtained analyzing data sets with [Chla] < 10 mg m^{-3}, where the variability of a_{Chla}^* appears to increase (Fig. 4 and Refs. 12 and 48).

Table 2. Intercepts (a_0) and slopes (a_1) with Corresponding Standard Errors (STE), Standard Errors of Estimate, and Coefficients of Determination (r^2) for Linear Regressions of Different Versions of the Model Obtained Using the Development Data Set[a]

Band Combination	a_0(STE)	a_1(STE)	STE of Estimate (mg m^{-3})	r^2
$R_{rs}^{-1}(673)R_{rs}(735)$	−15 (2)	94 (2.5)	8.6	0.95
$R_{rs}^{-1}(665)R_{rs}(725)$	−23 (2)	70 (2)	8.4	0.95
$[R_{rs}^{-1}(671) - R_{rs}^{-1}(710)]R_{rs}(740)$	16 (1)	125 (3)	8.7	0.94
$R_{rs}^{-1}(675)R_{rs}(705)$	−47 (5)	53 (3)	17.8	0.77
Reflectance height	–	28 (2)	29.9	0.34

[a]Only significant ($p < 0.001$) parameters were reported. All relationships were significant at the level $p < 0.0001$. The number of samples was 86.

Table 3. Descriptive Statistics of the Coefficient of Variation (%) Obtained Estimating [Chla] Using the Six Replicate Reflectance Spectra Collected at Each Station, and Different Models Versions with the a_0 and a_1 Coefficients Presented in Table 2 ($N = 100$)

Band Combination	Average	St. Dev.	Median	Min	Max
$R_{rs}^{-1}(673)R_{rs}(735)$	8.6	9.0	5.1	0.5	40.0
$R_{rs}^{-1}(665)R_{rs}(725)$	7.2	11.9	3.1	0.4	87.2
$[R_{rs}^{-1}(671) - R_{rs}^{-1}(710)]R_{rs}(740)$	4.3	5.6	1.9	0.3	32.6
$R_{rs}^{-1}(675)R_{rs}(705)$	7.5	8.4	5.0	0.5	54.9
Reflectance height	7.3	6.6	5.3	0.6	36.4
Gons, 1999	4.7	6.0	2.4	0.3	41.5

3. Parameterization

After having identified the optimal spectral bands for our models, we calculated the calibration coefficients of the best-fit linear function between several versions of the models and [Chla] (Table 2, Fig. 8). We also calculated the widely used reflectance ratio $R_{rs}^{-1}(675)R_{rs}(705)$ (Refs. 1–3 and the reflectance height above the baseline between 670 and 740 nm (Ref. 8).

The models Y and Z were strongly correlated to [Chla] ($r^2 \sim 0.94$), when we used reflectance bands located in the spectral regions where the interferences owing to variations in $a_{Chla}*$ and η were minimal. On the other hand, Z with $\lambda_1 = 675$ nm and $\lambda_3 = 705$ nm explained a smaller part of the [Chla] variance ($r^2 = 0.77$) because a spectral region of higher sensitivity to the interfering factors was encountered.

The reflectance height above the baseline showed the minimum coefficient of determination (0.34). It
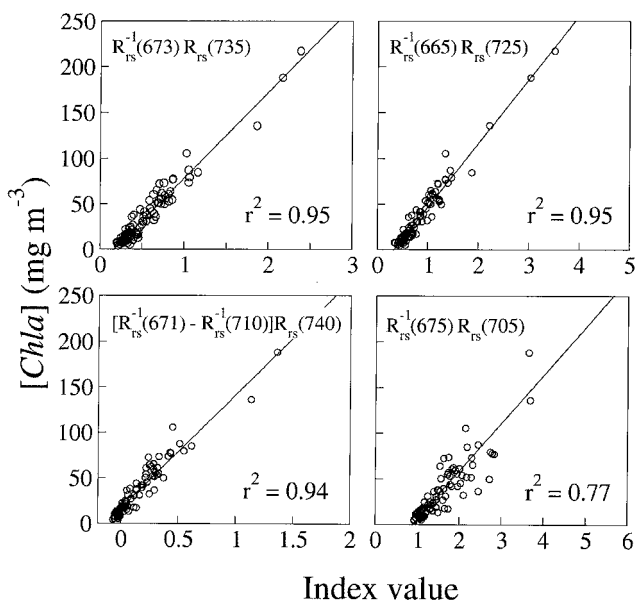

Fig. 8. Scatter plots of different versions of the model versus [Chla] measured analytically. The solid lines are the linear-regression fits. Coefficients of determination are also reported for each plot.

was considerably affected by the variability in backscattering among samples.

C. Precision

To assess the precision of the technique, we exploited the six replicate reflectance spectra measured at each station. For each spectrum, we estimated [Chla], using the coefficients a_0 and a_1 presented in Table 2. The precision was quantified as the coefficient of variation of the estimated [Chla] at each station. We also compared the precision of our model and band ratios with Gons's algorithm (hereinafter abbreviated as G99).[5] To do so, we converted our R_{rs} measurements into just-below surface-irradiance reflectance spectra as $R(0^-) = R_{rs}(n^2/t)Q(1 - \rho)$, where $Q = 3.38$ and $\rho = 0.02$ (where ρ is the Fresnel reflectance, Ref. 5). G99 uses three spectral channel located at 672, 704, and 776 nm. Part of the reflectance spectra were noisy at 776 owing to a decrease in the sensitivity of our radiometers in this spectral region; therefore we removed noisy stations by using the following criterion. Since the absorption coefficient of water is higher at 840 nm than at 750 nm, then $R(750)$ must be higher than $R(840)$. Thus we discarded all stations for which $R(840) > R(750)$ (of the initial 144 stations, 100 met this criterion). Then, to compute [Chla], we set $a_{Chla}*(672) = 0.0176$ m^2 mg^{-1} and $p = 1.065$ (where p is a calibration factor, see Ref. 5).

Descriptive statistics of the [Chla] coefficient of variation for the whole data set, after application of the above filtering, are presented in Table 3. The median values of the coefficients of variation were found between 1.9% and 5.3%, indicating that the measurement technique was characterized by satisfactory precision. The smallest median (1.9%) and maximal coefficients of variation (32.6%) were found for the three-band model $[R_{rs}^{-1}(671) - R_{rs}^{-1}(710)]R_{rs}(740)$. The major source of this variability was the depth under the surface at which the optical fiber was kept to measure the upward radiance. Under windy conditions, it was difficult to keep it as a constant depth, and its oscillations determined the precision interval; in the worst conditions, the coefficients of variation reached values as high as 87%.

Table 4. Results of the Model Validation[a]

Band Combination	a_0(STE)	a_1(STE)	RMSE of [Chla] Prediction (mg m^{-3})	RMS	RMS$_{>10}$	r^2
$R_{rs}^{-1}(673)R_{rs}(673)R_{rs}(735)$	−8 (3)	0.99 (0.04)	13.7	0.40	0.30	0.91
$R_{rs}^{-1}(665)R_{rs}(725)$	−9 (3)	1.04 (0.04)	14.2	0.47	0.36	0.91
$[R_{rs}^{-1}(675)R_{rs}(705)]$	–	0.93 (0.03)	15.1	0.45	0.25	0.88
$R_{rs}^{-1}(675)R_{rs}(705)$	−13 (5)	**1.31** (0.08)	28.3	0.71	0.48	0.84
Reflectance height	13 (4)	**0.55** (0.06)	28.5	0.48	0.43	0.57
Gons, 1999	−23 (10)	**2.31** (0.16)	77.1	0.77	0.76	0.74

[a]a_0 and a_1 are the intercepts and slopes (with corresponding standard errors in brackets), respectively, of the best linear fits between observed and predicted [Chla] values. RMSE is the root-mean-square error. RMS is the relative RMSE; RMS$_{>10}$ is the RSM computed excluding stations with [Chla] < 10 mg m^{-3}. Slopes in bold were significantly different from one ($p < 0.05$). Only intercepts significantly different from zero ($p < 0.05$) were included. The number of samples was 58.

D. Algorithm Validation

The result of the validation procedure, which was carried out using the independent-validation data set, are summarized in Table 4 and Fig. 9. The most accurate predictions of [Chla] were obtained when the bands used in the models Z and Y were selected to avoid interferences by variations in η and a_{Chla}*, i.e., for $R_{rs}^{-1}(673)R_{rs}(735)$, $R_{rs}^{-1}(665)R_{rs}(725)$ $[R_{rs}^{-1}(671) - R_{rs}^{-1}(710)]R_{rs}(740)$. The slopes of the observed [Chla] versus predicted [Chla] were not significantly different from one ($p > 0.05$), the root-mean-square error (RMSE) was approximately 15 mg m^{-3}, and the relative RMSE (RMS) was between 40% and 45% (Table 4).

The predictive performance of the $R_{rs}^{-1}(675)R_{rs}(705)$ ratio was lower: The slope (1.33) and intercept (-13 mg m^{-3}) of the observed [Chla] versus predicted [Chla] were significantly different

($p > 0.05$) from one and zero, respectively; the RMSE of [Chla] prediction was 28.3 mg m^{-3}, the RMS ~ 0.48. This loss of accuracy occurs because the bands used in this model are strongly affected by uncertainties that can be related to the variability of η and a_{Chla}* [Figs. 6(b) and 6(d)].

The reflectance height above the baseline yielded the poorest result because it was affected by the variability in backscattering between samples. Its weak predictive potential is well described by the coefficient of determination (0.57) and RMS (0.48), as well as by the slope (0.55) and intercept (13) of the observed [Chla] versus predicted [Chla] line that were significantly different from one and zero ($p < 0.05$), respectively. This limitation is likely to apply for most models based on absolute values of reflectance.

G99 yielded the largest RMSE (77.1 mg m^{-3}) and consistently overestimated [Chla]: The slope of the observed [Chla] versus predicted [Chla] was 2.31. Because we measured an average (± 1 standard deviation) a_{Chla}*(672) $= 0.022 \pm 0.007$ m^2 mg^{-1}, we repeated the calculations using this value and obtained a RMSE $= 56.7$ mg m^{-3} and a slope of 1.85. This improved prediction of [Chla] obtained with higher values of a_{Chla}* indicates that G99 is sensitive to variations in a_{Chla}* and therefore requires *in situ* calibration.

An analysis of the residuals of the regressions presented in Fig. 9 indicated that the largest relative departures from the 1:1 line occurred for [Chla] lower than 10 mg m^{-3}, often yielding negative [Chla] predictions in the case of the band ratios. Exclusion of the eight stations (three for G99) with [Chla] < 10 mg m^{-3}, improved the performance of the models: In the case of the three-band model, the RSM decreased to 0.25 (Table 4).

5. Conclusions

In this study, we presented the analytical development and the underlying hypotheses of a three-band remote-sensing algorithm for estimating [Chla] in turbid productive waters. NIR-to-red reflectance ratios can be seen as a special case of this model. We demonstrated that the variability of ecophysiological parameters, such as the
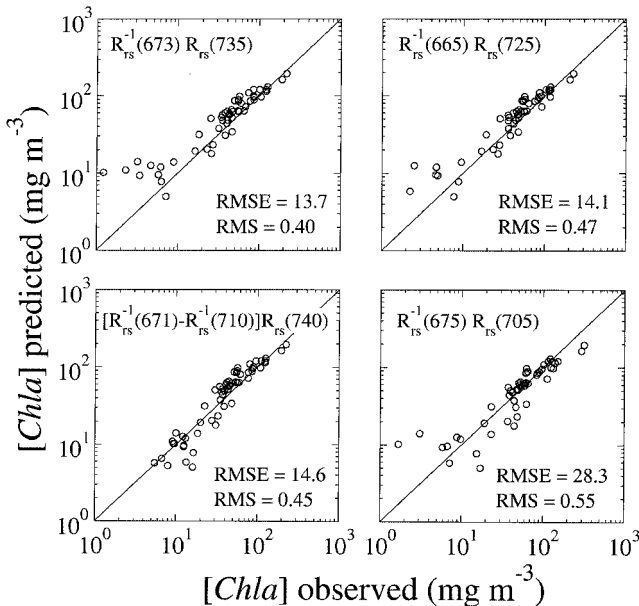

Fig. 9. Validation scatter plots for different versions of the model. The solid lines represent the 1-to-1 lines. Root-mean-square errors (RMSE), in mg m^{-3}) and relative root-mean-square errors (RMS) are also reported in each plot.

Chla fluorescence quantum yield and the Chla specific absorption coefficient, affects the remote estimation of [Chla]. The parameterization of $a_{\text{Chla}}*$ and η requires *a priori* knowledge of many different variables such as phytoplankton cell-size distribution, intracellular pigment content, temperature, and nutrient concentrations. Instead of attempting to model these interferences, we proposed to tune the model band positions in order to minimize these effects.

We analyzed a series of experimental observations gathered during different seasons over a two-year period, in turbid productive lakes of different origins. We showed that both η and $a_{\text{Chla}}*$ varied widely, thus potentially influencing the accuracy of remote estimates of [Chla]. Tuning the spectral regions used in the three-band model and in band ratios allowed us to accurately predict [Chla]. It was found that, to minimize these interferences, one should either set λ_1 = 673 nm and $\lambda_3 >$ 730 nm, or λ_3 = 705 and λ_1 ~ 665 nm. This is consistent with the results of other empirical studies.[49–55] In terms of accuracy, the three-band model was not considerably different from appropriately tuned band ratios yielding RMS around 0.30 (Table 4). However, it was characterized by the highest precision (~2%, Table 3).

The largest relative errors of [Chla] prediction were found for [Chla] values below 10 mg m^{-3}, as it was also reported in other studies.[4,5] We believe that the main reasons for these discrepancies may be the following: (a) The models are optimized for moderate to high Chla concentrations (mean [Chla] = 46 mg m^{-3}, Table 1); (b) the Chla specific absorption coefficient near the Chla red-absorption maximum showed its maximal variability for [Chla] below 10 mg m^{-3}; (c) our initial hypothesis regarding f/Q may not hold for the low [Chla] range; and (d) when [Chla] < 10 mg m^{-3}, R_{rs} values in the NIR may be too low and thus affected by larger measurement uncertainties.

We recognize that the results of the spectral tuning of the model and the calibration coefficients that we obtained depend on optical characteristics of water bodies studied. They should be considered valid only for the ranges of optically active constituents presented here. However, the large range of the optically active constituents sampled supports the robustness of the proposed model and of our analysis.

References

1. A. A. Gitelson and K. Y. Kondratyev, "Optical models of mesotrophic and eutrophic water bodies," Int. J. Remote Sens. **12,** 373–385 (1991).

2. A. A. Gitelson, G. Garbuzov, F. Szilagyi, K.-H. Mittenzwey, A. Karnieli, and A. Kaiser, "Quantitative remote sensing methods for real time monitoring of inland water quality," Int. J. Remote Sens. **14,** 1269–1295 (1993).

3. A. G. Dekker, "Detection of optical water quality parameters for eutrophic waters by high resolution remote sensing," Ph.D. thesis (Vrije Universiteit, Amsterdam, The Netherlands, 1993).

4. H. J. Gons, M. Rijkeboer, and K. G. Ruddick, "A chlorophyll-retrieval algorithm for satellite imagery (Medium Resolution Imaging Spectrometer) of inland and coastal waters," J. Plankton Res. **24,** 947–951 (2002).

5. H. J. Gons, "Optical teledetection of chlorophyll a in turbid inland waters," Environ. Sci. Technol. **33,** 1127–1132 (1999).

6. H. J. Gons, M. Rijkeboer, S. Bagheri, and K. G. Ruddick, "Optical teledetection of chlorophyll a in estuarine and coastal waters," Environ. Sci. Technol. **34,** 5189–5192 (2000).

7. K. G. Ruddick, H. J. Gons, M. Rijkeboer, and G. Tilstone, "Optical remote sensing of chlorophyll a in case 2 waters by use of an adaptive two-band algorithm with optimal error properties," Appl. Opt. **40,** 3575–3585 (2001).

8. A. A. Gitelson, M. Mayo, Y. Z. Yacobi, A. Parparov, and T. Berman, "The use of high-spectral-resolution radiometer data for detection of low chlorophyll concentrations in Lake Kinneret," J. Plankton Res. **16,** 993–1002 (1994).

9. J. F. R. Gower, "Observations of *in-situ* fluorescence of chlorophyll-*a* in Saanich Intel," Boundary-Layer Meteorol. **18,** 235–245 (1980).

10. R. A. Neville and J. F. R. Gower, "Passive remote sensing of phytoplankton via chlorophyll α fluorescence," J. Geophys. Res. **82,** 3487–3493 (1977).

11. J. F. R. Gower, R. Doerffer, and G. A. Borstad, "Interpretation of the 685 nm peak in water-leaving radiance spectra in terms of fluorescence, absorption and scattering, and its observation by MERIS," Int. J. Remote Sens. **20,** 1771–1786 (1999).

12. A. Bricaud, M. Babin, A. Morel, and H. Claustre, "Variability in the chlorophyll-specific absorption-coefficients of natural phytoplankton: analysis and parameterization," J. Geophys. Res. [Oceans] **100,** 13321–13332 (1995).

13. M. Babin, A. Morel, and B. Gentili, "Remote sensing of sea surface sun-induced chlorophyll fluorescence: consequences of natural variations in the optical characteristics of phytoplankton and the quantum yield of chlorophyll a fluorescence," Int. J. Remote Sens. **17,** 2417–2448 (1996).

14. D. A. Kiefer and R. A. Reynolds, "Advances in understanding phytoplankton fluorescence and photosynthesis," in *Primary Productivity and Biogeochemical Cycles in the Sea,* P. G. Falkowsky and A. D. Woodhead, eds. (Plenum, New York, 1992).

15. G. Dall'Olmo, A. A. Gitelson, and D. C. Rundquist, "Towards a unified approach for remote estimation of chlorophyll-a in both terrestrial vegetation and turbid productive waters," Geophys. Res. Lett. **30,** 1938, doi:10.1029/2003GL018065 (2003).

16. A. A. Gitelson, Y. Gritz, and M. N. Merzlyak, "Relationship between leaf chlorophyll content and spectral reflectance and algorithms for non-destructive chlorophyll assessment in higher plant leaves," J. Plant Physiol. **160,** 271–282 (2003).

17. Z. P. Lee, K. L. Carder, S. K. Hawes, R. G. Steward, T. G. Peacock, and C. O. Davis, "Model for the interpretation of hyperspectral remote-sensing reflectance," Appl. Opt. **33,** 5721–5732 (1994).

18. H. R. Gordon, O. B. Brown, R. H. Evans, J. W. Brown, R. C. Smith, K. S. Baker, and D. K. Clark, "A semianalytic radiance model of ocean color," J. Geophys. Res. **93,** 10909–10924 (1988).

19. K. L. Carder and R. G. Steward, "A remote-sensing reflectance model of a red-tide dinoflagellate off West Florida," Limnol. Oceanogr. **30,** 286–298 (1985).

20. A. Morel and B. Gentili, "Diffuse reflectance of oceanic waters: its dependence on sun angle as influenced by the molecular-scattering contribution," Appl. Opt. **30,** 4427–4438 (1991).

21. A. Morel and B. Gentili, "Diffuse-reflectance of oceanic waters. 2. Bidirectional aspects," Appl. Opt. **32,** 6864–6879 (1993).

22. H. Loisel and A. Morel, "Nonisotropy of the upward radiance field in typical coastal (case 2) waters," Int. J. Remote Sens. **22,** 275–295 (2001).

23. F. Melin, G. Zibordi, and J. F. Berthon, "Assessment of SeaWiFS atmospheric and marine products for the Northern Adriatic Sea," IEEE Trans. Geosci. Remote Sens. **41,** 548–558 (2003).

24. T. Heege, "Flugzeuggestützte Fernerkundung von Wasserinhaltsstoffen am Bodensee," Ph.D. thesis (DLR-Forschungsbericht, Wessling, Germany, 2002).

25. C. S. Roesler, M. J. Perry, and K. L. Carder, "Modeling *in situ* phytoplankton absorption from total absorption spectra in productive inland marine waters," Limnol. Oceanogr. **34,** 1510–1523 (1989).

26. A. Bricaud, A. Morel, and L. Prieur, "Absorption by dissolved organic matter of the sea (yellow substance) in the UV and visible domains," Limnol. Oceanogr. **1,** 43–53 (1981).

27. J. T. O. Kirk, *Light and Photosynthesis in Aquatic Ecosystems* (Cambridge University, Cambridge, UK, 1994).

28. M. Babin and D. Stramski, "Light absorption by aquatic particles in the near-infrared spectral region," Limnol. Oceanogr. **47,** 911–915 (2002).

29. C. D. Mobley, *Light and Water: Radiative Transfer in Natural Waters* (Academic, San Diego, Calif., 1994).

30. N. A. Welschmeyer, "Fluorometric analysis of chlorophyll *a* in the presence of chlorophyll *b* and pheopigments," Limnol. Oceanogr. **39,** 1985–1992 (1994).

31. American Public Health Association, American Water Works Association, and Water Pollution Control Federation, *Standard Methods for the Examination of Water and Wastewater* (American Public Health Association, Washington, D.C., 1989).

32. S. Tassan and G. M. Ferrari, "An alternative approach to absorption measurements of aquatic particles retained on filters," Limnol. Oceanogr. **40,** 1358–1368 (1995).

33. G. S. Fargion and J. L. Mueller, "Ocean optics protocols for SeaWiFS validation, revision 2," NASA Tech. Memorandum 2000-209966 (NASA Goddard Space Flight Center, Greenbelt, Maryland, 2000).

34. G. B. Mitchell, "Algorithms for determining the absorption coefficient of aquatic particulates using the quantitative filter technique (QFT)" in *Ocean Optics X* (SPIE, Bellingham, Wash., 1990).

35. A. Morel and L. Prieur, "Analysis of variations in ocean color," Limnol. Oceanogr. **22,** 709–722 (1977).

36. A. A. Gitelson, "The peak near 700 nm on radiance spectra of algae and water: relationships of its magnitude and position with chlorophyll concentration," Int. J. Remote Sens. **13,** 3367–3373 (1992).

37. A. Vasilkov and O. Kopelevich, "Reasons for the appearance of the maximum near 700 nm in the radiance spectrum emitted by the ocean layer," Oceanology **22,** 697–701 (1982).

38. P. Pringsheim, *Fluorescence and Phosphorescence* (Interscience, New York, (1949).

39. P. G. Falkowski and J. A. Raven, *Aquatic Photosynthesis* (Blackwell, Malden, Massachusetts, 1997).

40. K. Allali, A. Bricaud, and H. Claustre, "Spatial variations in the chlorophyll-specific absorption coefficients of phytoplankton and photosynthetically active pigments in the equatorial pacific," J. Geophys. Res. [Oceans] **102,** 12413–12423 (1997).

41. S. E. Lohrenz, A. D. Weidemann, and M. Tuel, "Phytoplankton spectral absorption as influenced by community size structure and pigment composition," J. Plankton Res. **25,** 35–61 (2003).

42. D. Stramski, A. Sciandra, and H. Claustre, "Effects of temperature, nitrogen, and light limitation on the optical properties of the marine diatom Thalassiosira Pseudonana," Limnol. Oceanogr. **47,** 392–403 (2002).

43. H. Claustre, A. Bricaud, M. Babin, F. Babin, F. Bruyant, L. Guillou, F. Le Gall, D. Marie, and F. Partensky, "Diel variations in prochlorococcus optical properties," Limnol. Oceanogr. **47,** 1637–1647 (2002).

44. T. Fujiki and S. Taguchi, "Variability in chlorophyll alpha specific absorption coefficient in marine phytoplankton as a function of cell size and irradiance," J. Plankton Res. **24,** 859–874 (2002).

45. H. Buiteveld, J. H. M. Hakvoort, and M. Donze, "The optical properties of pure water," in *Ocean Optics XII*, Proc. SPIE **2258,** 174–183 (1994).

46. V. E. Brando and A. G. Dekker, "The fluorescence term on the observed 690–710 nm reflectance peak in eutrophic turbid (inland) waters: myth or reality?" in *Ocean Optics XVI,* (Office of Naval Research, Santa Fe, New Mexico, 2002).

47. C. S. Roesler and M. J. Perry, "*In-situ* phytoplankton absorption, fluorescence emission, and particulate backscattering spectra determined from reflectance," J. Geophys. Res. [Oceans] **100,** 13279–13294 (1995).

48. A. Bricaud, A. Morel, M. Babin, K. Allali, and H. Claustre, "Variations of light absorption by suspended particles with chlorophyll *a* concentration in oceanic (case 1) waters: analysis and implications for bio-optical models," J. Geophys. Res. [Oceans] **103,** 31033–31044 (1998).

49. D. Pierson and N. Strömbäck, "A modelling approach to evaluate preliminary remote sensing algorithms: use of water quality data from Swedish great lakes," Geophysica **36,** 177–202 (2000).

50. K. Oki and Y. Yasuoka, "Estimation of chlorophyll concentration in lakes and inland seas with a field spectroradiometer above the water surface," Appl. Opt. **41,** 6463–6469 (2002).

51. E. F. Hoge and C. W. S. N. R. Wright, "Radiance-ratio algorithm wavelengths for remote oceanic chlorophyll determination," Appl. Opt. **26,** 2082–2094 (1987).

52. K. Kallio, T. Kutser, T. Hannonen, S. Koponen, J. Pulliainen, J. Veps, and T. Pyh, "Retrieval of water quality from airborne imaging spectrometry of various lake types in different seasons," Sci. Total Environ. **268,** 59–77 (2001).

53. J. Pulliainen, K. Kallio, K. Eloheimo, S. Koponen, H. Servomaa, T. Hannonen, S. Tauriainen, and M. Hallikainen, "A semi-operative approach to lake water quality retrieval from remote sensing data," Sci. Total Environ. **268,** 79–93 (2001).

54. K. Kallio, S. Koponen, and J. Pulliainen, "Feasibility of airborne imaging spectrometry for lake monitoring: a case study of spatial chlorophyll alpha distribution in two meso-eutrophic lakes," Int. J. Remote Sens. **24,** 3771–3790 (2003).

55. P. Ammenberg, P. Flink, T. Lindell, D. Pierson, and N. Strombeck, "Bio-optical modelling combined with remote sensing to assess water quality," Int. J. Remote Sens. **23,** 1621–1638 (2002).